PAPER

CrossMark
click for updates

Switching adsorption and growth behavior of ultrathin [C₂C₁Im][OTf] films on Au(111) by Pd deposition

F. Rietzler, B. May, H.-P. Steinrück and F. Maier*

Combining *in vacuo* deposition of ultrathin ionic liquid (UTIL) films with angle-resolved X-ray photo-electron spectroscopy (ARXPS), we demonstrate that by deposition of submonolayer amounts of Pd onto Au(111) the initial growth mode of the ionic liquid (IL) 1-ethyl-3-methylimidazolium trifluoro-methanesulfonate ([C₂C₁Im][OTf]) can be switched from three-dimensional (3D) to two-dimensional (2D) growth, that is, from non-wetting to wetting. On clean Au(111), pronounced 3D growth occurs on top of an initially formed 2D wetting layer with cations and anions next to each other in a checkerboard arrangement. After pre- or postdeposition of only 0.7 ML Pd, two-dimensional layer-by-layer growth is found, which is attributed to strong attractive interactions between [C₂C₁Im][OTf] and surface Pd. For Pd post deposition onto the IL, the ARXPS data revealed particularly strong interactions between the dialkylimidazolium cation and Pd atoms, which considerably reduce the regular surface alloying of Pd with the Au substrate stabilizing Pd at the metal surface. In the context of heterogeneous catalysis using the SCILL (solid catalyst coated with ionic liquid layer) concept, these results directly provide a possible explanation on the molecular level for the beneficial influence of the IL layer in case of heterogeneous metal alloy catalysts.

1. Introduction

Ionic liquids (ILs) are entirely ionic compounds exhibiting a comparatively low melting point, which often lies even below room temperature (RT). Besides their application as a novel class of solvents in synthesis[1,2] and as electrolytes in electro-chemical devices,[3–8] the extremely low vapor pressure of ILs led to the development of completely new thin film concepts in catalysis:[9] solid catalyst with ionic liquid layer (SCILL) and supported ionic liquid phase (SILP). The SILP concept is based on a porous inert support material coated with a thin IL layer containing the homogeneously dissolved catalyst. SILP thus combines the advantages of homogenous catalysis (highly product- and stereo-selective) and heterogeneous catalysis (stationary catalyst phase in a continuous flow reactor). In SCILL, a thin IL layer covers the solid porous material, which itself is a catalyst or is decorated with catalytically active species such as nanoparticles. By specific interactions of the IL with reactive sites of the heterogeneous catalyst or by solubility and mass transport changes of reactants and products through the IL layer to/from the catalyst surface, the IL is able to enhance selectivity, product distribution, and yields in these SCILL systems.[9]

Lehrstuhl für Physikalische Chemie II, Friedrich-Alexander-Universität Erlangen-Nürnberg, Egerlandstr. 3, 91058 Erlangen, Germany. E-mail: florian.maier@fau.de

For many high surface area applications, the structure and composition of the IL/solid interface are of great interest. Of particular importance in the context of SILP and SCILL are the adsorption and wetting properties of the IL on different substrates, due to the thin IL film impregnation technologies involved. A detailed understanding of these interface properties will allow for tailoring systems for specific applications.[9] Hence, during the last years, the IL/solid interface has drawn increasing attention and has been studied with numerous techniques including sum frequency generation (SFG),[10,11] scanning tunneling microscopy (STM),[12–14] atomic force micro-scopy (AFM),[13,15] neutron reflectometry,[16] and X-ray photo-electron spectroscopy (XPS).[12,17–20] In our previous studies of the IL/solid interface, ultrathin IL (UTIL) films were deposited onto different supports *via* physical vapor deposition (PVD)[17] or electrospray ionization deposition (ESID)[21] and analyzed by means of angle-resolved XPS (ARXPS). Driven by the complex interplay of interionic IL–IL as well as IL–support interactions, different combinations of ILs and supports show very different behavior concerning initial adsorption and subsequent IL growth. Upon *in vacuo* deposition of dialkyl-imidazolium and -pyrrolidinium ILs, such as [C₁C₁Im][Tf₂N], [C₈C₁Im][Tf₂N], and [C₄C₁Pyr][Tf₂N], a specific surface arrangement is found on Au(111).[12,18] These ILs, which all contain weakly coordinating [Tf₂N]⁻ anions, first form a closed layer on the Au(111) substrate.

At room temperature, ARXPS unequivocally shows that within this closed layer, the anions and cations are both in direct contact with the metal surface, which we refer to the so-called checkerboard arrangement.[18] Note that at room temperature, the ions are still highly mobile within this ion layer forming a 2D liquid state as proven by STM.[12] At temperatures well below 200 K, this layer freezes into crystalline and – depending on cooling conditions – amorphous domains, which even allows for imaging with STM the individual cations and anions sitting both next to each other at the Au(111) surface. Depending on tunneling conditions, the herringbone reconstruction of the Au(111) surface underneath this IL layer is still visible at low and also at room temperature, which indicates that the IL ions are only weakly interacting with the gold surface atoms.[12] ARXPS also revealed two-dimensional (2D) layer-by-layer growth up to at least 10 ML during subsequent deposition of these ILs on Au(111).[18,21] A completely different behavior was observed for $[C_1C_1Im][Tf_2N]$ deposited onto Ni(111).[19] In the submonolayer regime, the IL was found to adsorb with the imidazolium cation in contact with the nickel surface and the $[Tf_2N]^-$ anion on top of it; this so-called sandwich arrangement is likely driven by attractive $[C_1C_1Im]^+$-Ni interactions. Upon further IL deposition, a gradual transition to a checkerboard configuration of alternately oriented ion pairs was observed, forming a wetting layer of one monolayer (ML) thickness; this transition is attributed to repulsive dipole–dipole interactions of neighboring ion sandwiches. For coverages above 1 ML, ARXPS revealed the onset of three-dimensional (3D) island growth on top of the initially formed wetting layer.[19] The same IL, $[C_1C_1Im][Tf_2N]$, deposited onto mica or carbonaceous supports already exhibits pronounced three-dimensional (3D) growth characteristics from the very beginning, which is attributed to very weak IL–substrate interactions.[20,22] For $[C_8C_1Im]Cl$ deposited onto Au(111), first, a strongly bound checkerboard wetting layer of 0.5 ML thickness with highly oriented octyl chains pointing towards vacuum was detected; subsequent IL deposition of $[C_8C_1Im]Cl$ on top of this alkyl carbon surface again revealed pronounced three-dimensional IL island growth.[21] All these studies thus provide clear evidence that thin film interfaces strongly depend on the nature of IL–IL and IL–substrate interactions. Nevertheless, a fundamental understanding of the factors driving a particular behavior is still missing.

One important question in this context now is, whether and how the adsorption and wetting behavior of ILs on different substrates can be modified, e.g., by the pre- or postadsorption of other substances. One example for a molecular adsorbate is cyclohexane on Ni(111), which can be switched from wetting to non-wetting by preadsorption of 0.34 ML potassium.[23] Similarly important is the reverse influence of the IL layer on the catalytic properties of the solid catalyst surface in SCILL systems, particularly, when near-surface alloys[24] of noble metal/transition metal catalysts such as Au/Pd alloys are involved. Ensemble effects (that is, a specific geometric configuration at the alloy surface, required for facilitating a particular catalytic process) and ligand effects (that is, the electronic modification of the catalytically active surface atoms by their environment)[25] can be influenced by additional interactions of the metal atoms with

the IL layer. Pd is known to form surface alloys with Au preferentially enriched at the surface[26] even at RT.[27] In case of Pd slowly deposited onto the reconstructed Au(111) surface at room temperature, STM revealed that small metal islands first started to grow in the elbows of the herringbone reconstruction with partially exchanging Au surface sites by Pd atoms from the very beginning. Increasing surface strain by further Pd deposition eventually led to the disruption of the gold surface reconstruction for Pd coverages above 0.25 ML.[28] Concerning the interaction of Pd and imidazolium-based ILs, as employed in this work, Pd of different oxidation states is known to efficiently form stable N-heterocyclic carbenes, which are active in case e.g. of homogeneously or heterogeneously catalyzed Heck and Suzuki coupling reactions.[29] Imidazolium-based ILs have a tendency, particularly under basic conditions, forming neutral carbene species as intermediates in catalytic reactions; Pd–carbene complexes generated from imidazolium cations are thus used in organic reactions as well (for a review on the non-innocent role of ILs in catalysis, see the work of Chowdhury et al.[30]). With respect to metallic palladium, several surface science studies have shown that $[C_nC_1Im][OTf]$ ILs strongly exhibit attractive interactions with alumina-supported Pd nanoparticles via the sulfonate group of the anion and the C_2-position of the imidazolium cation.[31,32] One thus might envision that these attractive Pd–IL interactions could lead to a stabilization of Pd at the solid–liquid interface in case of gold–palladium surface alloys, and thus, to an interface-enrichment of Pd compared to the system without IL. In the extreme case, it is furthermore well possible under certain reaction conditions, that these attractive interactions even transform a SCILL catalyst to a SILP-like system by dissolution of active species from the solid surface into the IL film.[9]

To obtain a better understanding of the factors driving the initial adsorption and wetting properties and in the search for possible ways for switching between different behaviors, we investigated the influence of Pd on the adsorption and growth behavior of UTIL $[C_2C_1Im][OTf]$ films deposited on Au(111). This material combination also is of interest for real hydrogenation SCILL catalysts, with high activity and selectivity.[31,32] Both Pd and IL were thermally deposited onto the gold substrate by means of PVD. Au(111) was chosen for best comparability with our previous studies on the IL/metal interface.[18,21] The influence of Pd on the adsorption and growth properties of the IL were studied with two different experimental approaches, that is, Pd was either deposited prior or subsequent to the deposition of the IL.

2. Experimental

The Au(111) single crystal with a size of $11 \times 11 \times 2$ mm^3 was purchased from MaTecK (purity 99.999%, one side polished and aligned to the (111) plane with an accuracy better than 0.1°). It was mounted onto a Mo sample holder and fixed with two Ta wires. Surface preparation was performed by sputtering

25144 | Phys. Chem. Chem. Phys., 2016, **18**, 25143–25150

This journal is © the Owner Societies 2016

with 1.0 keV Ar$^+$ ions, followed by annealing at $\sim$800 K. Sample cleanliness was checked by XPS.

1-Ethyl-3-methylimidazolium trifluoromethanesulfonate ([C$_2$C$_1$Im][OTf], see inset of Fig. 3) was synthesized and dried according to previous work.[32] UTIL films – that is, IL films with a total mean thickness below 5 nm, and thus, only a small number of molecular layers in case of a two-dimensional film morphology – were prepared by PVD using a modified high-temperature Knudsen cell for organic materials (Tectra WKC3) onto the substrate kept at RT. In order to minimize influence of radiation damage, only three consecutive IL deposition steps were performed at once; in most cases, deposition was done on a freshly prepared Au(111) surface. The evaporation temperature of the Knudsen cell was regulated to a temperature of 440 K by an Eurotherm 2261 controller with an accuracy of $\pm$1 K, using a type-K thermocouple. The IL flux was checked using a quartz crystal microbalance (QCM) before and after each deposition step. The QCM was calibrated by deposition of the IL onto an Au(111) single crystal before and after each deposition series. Detailed information on the experimental setup can be found in one of our previous publications.[18]

Pd was evaporated with a Focus EFM 3 electron beam evaporator, which was mounted to the preparation chamber of the UHV system. For Pd deposition, electrons were accelerated towards a positively biased Pd rod (+0.95 keV, 11.2 mA) from a surrounding tungsten filament. Heat radiation was adsorbed by a water-cooled shroud; throughout the deposition procedure, the pressure inside the preparation chamber did not exceed 1 $\times$ 10^{-9} mbar. The evaporator's distance from the sample was chosen to be large enough to ensure the homogeneous deposition of Pd across the sample. In order to avoid additional surface defects caused by accelerated Pd ions present in the EFM metal flux, the Au crystal was positively biased with +1 kV $vs.$ ground. Deposition time was controlled by a manual built-in shutter. Prior to the experiments, the Pd flux was calibrated by QCM and by XPS. For this purpose, Pd was deposited onto a clean Au(111) single crystal and the attenuation of Au 4f substrate signals was monitored upon Pd deposition. Before and after each deposition, the Pd flux was checked for constancy by QCM. Additionally, during deposition, the integral flux monitor of the EFM evaporator was used for real-time control of constant deposition rate. Pd is known to form surface alloys with Au even at RT;[27] thus, only normal emission spectra with the corresponding large XPS information depth were used for calibrating the overall Pd flux (further details, see next section).

The XP spectra were measured with a VG Scienta R3000 electron analyzer and a SPECS XR 50 X-ray gun using non-monochromatized Al-Kα radiation ($h\nu$ = 1486.6 eV) at a power of 250 W (U = 12.5 kV, I = 20 mA). The core level spectra were recorded with a PE of 100 eV (overall resolution FWHM: $\sim$0.9 eV). The inelastic mean free path (IMFP) of photoelectrons with energies between 800 and 1300 eV in organic matter is 2–3 nm.[33] Consequently, the information depth (ID) of 0° measurements corresponds to 7–9 nm, that is, several molecular layers. In the more surface sensitive geometry at 80°, the ID is reduced by a factor of cos(80°) $\sim$ 1/6 down to 1–1.5 nm.[18]

To account for an overall reduction in intensity at grazing emission, all 80° spectra shown in this work were multiplied by an empirical factor which was determined by measurements of macroscopic films of the respective ILs under identical conditions as described somewhere else.[34] [C$_2$C$_1$Im][OTf] reference XP spectra were measured using a macroscopically thick film, which was prepared ex $situ$ by spreading about 0.1 ml of the IL onto a polycrystalline Au foil under ambient conditions. For quantification, all IL spectra were fitted with a Voigt profile (30% Lorentzian contribution) after a Shirley background subtraction.

In case of a two-dimensional homogeneous IL film of thickness d, the attenuation of the Au 4f substrate signal follows eqn (1), neglecting elastic scattering effects:

$$\frac{I_{d(n)}}{I_0} = e^{\frac{-d(n)}{\lambda \cdot \cos \theta}} \quad \text{or} \quad d(n) = \lambda \cos \theta \cdot \ln \frac{I_0}{I_{d(n)}} \qquad (1)$$

with λ being the inelastic mean free path (IMFP), $d(n)$ the total film thickness of n completed layers, and θ the emission angle with respect to the surface normal. For Au 4f electrons with a kinetic energy of $\sim$1400 eV, λ equals 3 nm.[33] In line with earlier publications, the UTIL film thicknesses are given in monolayers (ML); thereby 1 ML of IL refers to one closed layer of ion pairs with anions and cations on top of each other. The height h of 1 ML is estimated from the bulk molecular volume V_m, as derived from the IL's molar mass M and its mass density ρ, using eqn (2),

$$h = \sqrt[3]{\frac{V_m}{N_A}} = \sqrt[3]{\frac{M}{N_A \cdot \rho}} \qquad (2)$$

with N_A being the Avogadro constant. This approximation yields thicknesses (heights) of h_{IL} = 6.8 Å for 1 ML of [C$_2$C$_1$Im][OTf]. According to this definition of coverage, one single closed layer of cations and anions adsorbed next to each other in a so-called checkerboard configuration, corresponds to a coverage of 0.5 ML.[18] In order to study the IL growth on Au(111), the attenuation of the Au 4f substrate signal was determined at 0° and 80°. Eqn (2) was also applied to estimate on the height of 1 ML of Pd, resulting in h_{Pd} = 2.3 Å.

3. Results and discussion

3.1. [C$_2$C$_1$Im][OTf] on pristine Au(111)

In Fig. 1, the attenuation of the Au 4f substrate signals (I/I_0) at 0° and 80° upon deposition of [C$_2$C$_1$Im][OTf] onto Au(111) is plotted $versus$ nominal thickness, which was calculated from the calibrated flux of the PVD apparatus (see Experimental section). The blue (0°) and red (80°) dotted lines indicate attenuation for a homogeneously growing two-dimensional film according to eqn (1). Up to a nominal coverage of around 0.5 ML (3.4 Å; dashed black vertical line), at both emission angles, the attenuation of the Au 4f signal follows the dotted lines (blue for 0° and red for 80°), indicating a 2D layer-by-layer growth. This behavior indicates the formation of one closed ion layer in a checkerboard structure, with cations and anions
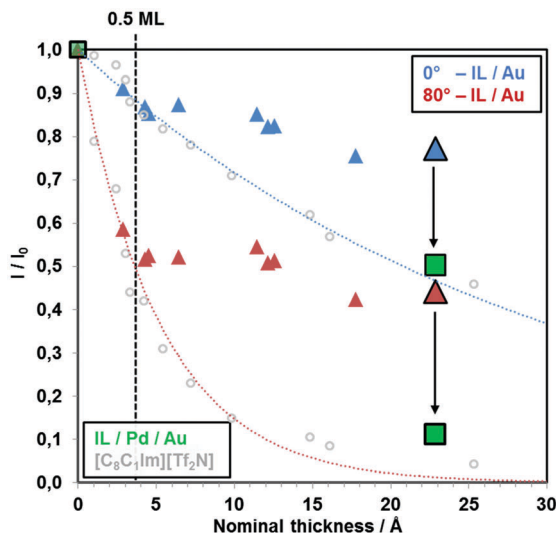
Fig. 1 Attenuation of the Au 4f substrate signal with increasing nominal $[C_2C_1Im][OTf]$ film thickness in $0°$ and $80°$ emission. The dotted curves represent the expected behavior for 2D layer-by-layer growth. 1 ML of $[C_2C_1Im][OTf]$ ion pairs corresponds to ~6.8 Å. The dashed line indicates an $[C_2C_1Im][OTf]$ coverage of 0.5 ML (= one closed ion layer in the checkerboard arrangement). For comparison, ARXPS data for the IL $[C_8C_1Im][Tf_2N]$ are also shown (grey open circles); this IL is known to grow in a layer-by-layer mode on Au(111).[18] Green squares show the attenuation of Au 4f intensity after deposition of ~23 Å $[C_2C_1Im][OTf]$ on Au(111) that was pre-covered with 1.6 Å (0.7 ML) Pd. All deposition steps were performed at RT.

adsorbed next to each other, with a coverage of 0.5 ML. Moreover, the atomic ratios of the measured IL signals (S 2p, C 1s, N 1s, O 1s, F 1s) determined by quantitative XPS analysis match the nominal IL stoichiometry within the margin of error ($\pm 10\%$), at $0°$ and also in surface sensitive $80°$ emission, ruling out the enrichment of one of the ionic species at the IL/vacuum interface. These findings imply the formation of a homogeneous wetting layer with a thickness of 0.5 ML, composed of anions and cations adsorbing next to each other in a checkerboard arrangement directly on Au(111).

For higher IL coverages, that is, above ~0.5 ML, a drastic change of the wetting behavior is observed. As seen in Fig. 1, the measured attenuation of the Au 4f signal is much less pronounced than for the ideal 2D behavior, that is, the data points lie significantly above the blue ($0°$) and red ($80°$) dotted lines. This behavior clearly indicates the formation of 3D islands, probably on top of the initially formed wetting layer. From our ARXPS data, however, we cannot completely rule out that the wetting layer breaks apart with increasing amount of IL, and three-dimensional IL islands are formed exposing partially the bare Au(111) surface. This growth behavior is very different to imidazolium $[Tf_2N]$ ILs, for which ideal layer-by-layer growth was observed for coverages up to at least 10 ML,[18,21] but resembles the growth of $[C_8C_1Im]Cl$ on the same substrate.[21]

A detailed discussion on factors such as interionic interaction strength influencing the growth mode of an IL was given in one of our previous publications[21] in order to explain the different morphologies of $[C_8C_1Im][Tf_2N]$ and $[C_8C_1Im]Cl$ thin

films deposited on Au(111). At first glance, the molecular structures of $[OTf]^-$ and $[Tf_2N]^-$ anions share obvious similarities. However, their corresponding interaction energies with a dialkyl-imidazolium cation differ drastically, as evaluated by Fernandes et al. in an ESI-MS/MS and quantum chemical calculation study. The dissociation energy of $[C_4C_1Im][OTf]$ was found to be 3.42 eV, which lies just in between the values determined for $[C_4C_1Im]Cl$ (3.85 eV) and $[C_4C_1Im][Tf_2N]$ (2.96 eV).[35] One reason for the higher dissociation energy of the $[OTf]^-$ anion compared to $[Tf_2N]^-$ is the smaller anion size, leading to an increase in hydrogen-bonding ability[36] and Coulomb interaction energy.[37] Hence, the relatively strong interionic interactions of $[C_2C_1Im][OTf]$ might lead to reduced IL–substrate interactions and consequentially provoke the observed 3D growth behavior on Au(111).

3.2. Influence of Pd deposition

In order to be able to study interfacial interactions of $[C_2C_1Im][OTf]$ with Pd by means of surface-sensitive XPS, only UTIL films with a nominal coverage of ~3 ML (which would correspond to a homogeneous film of 23 Å thickness) were deposited by PVD. Moreover, only very small nominal amounts of Pd in the sub-monolayer range were deposited by electron beam evaporation (1 ML Pd corresponds to ~2.3 Å). In the following, two experiments will be discussed with a different order of deposition.

In the first experiment, nominally 1.6 Å (~0.7 ML) of Pd were deposited onto clean Au(111) and subsequently 23 Å (~3 ML) of $[C_2C_1Im][OTf]$ on top (referenced to as "IL/Pd/Au"). In the second experiment, first nominally 23 Å of $[C_2C_1Im][OTf]$ were deposited onto clean Au(111) and subsequently 1.6 Å of Pd on top ("Pd/IL/Au"). Note that the normalized Au 4f signals at $0°$ and $80°$ in Fig. 1 after deposition of ~3 ML IL (23 Å; enlarged blue and red triangles, respectively) onto clean Au(111) lie significantly above the dashed lines for ideal 2D growth due to pronounced island formation.

For simplicity, the discussion on the Pd and Au signals will focus on the overlapping Pd 3d and Au 4d regions. Additional analysis of the separated Au 4f region was conducted (not shown), which was in perfect agreement with the results obtained for Au 4d. Furthermore, as the Au $4d_{5/2}$ signal coincides with the Pd $3d_{5/2}$ signal (~335 eV BE), only the Au $4d_{3/2}$ (~352 eV BE) and Pd $3d_{3/2}$ signals (~340.5 eV BE) will be discussed.

Fig. 2 shows $0°$ and $80°$ XP spectra of the Au 4d/Pd 3d region for the two deposition series. The black spectra correspond to the clean Au(111) surface. Upon the deposition of Pd onto clean Au(111) of the sequence "IL/Pd/Au", a decrease of the Au $4d_{3/2}$ intensity at 352 eV by ~9% is observed in normal emission, which is accompanied by the appearance of the Pd $3d_{3/2}$ signal at 340.5 eV in the orange spectra in Fig. 2(left). Application of eqn (1) to the attenuation of the Au $4d_{3/2}$ signal at $0°$ yields the expected thickness of the Pd layer of ~1.6 Å. In contrast, for the $80°$ data a nominal Pd layer thickness of only ~1.0 Å is calculated, resulting from a significantly lower attenuation than expected for a homogenous Pd adlayer. This effect is attributed to pronounced surface alloy formation of Pd with Au already discussed above, which was observed in a combined
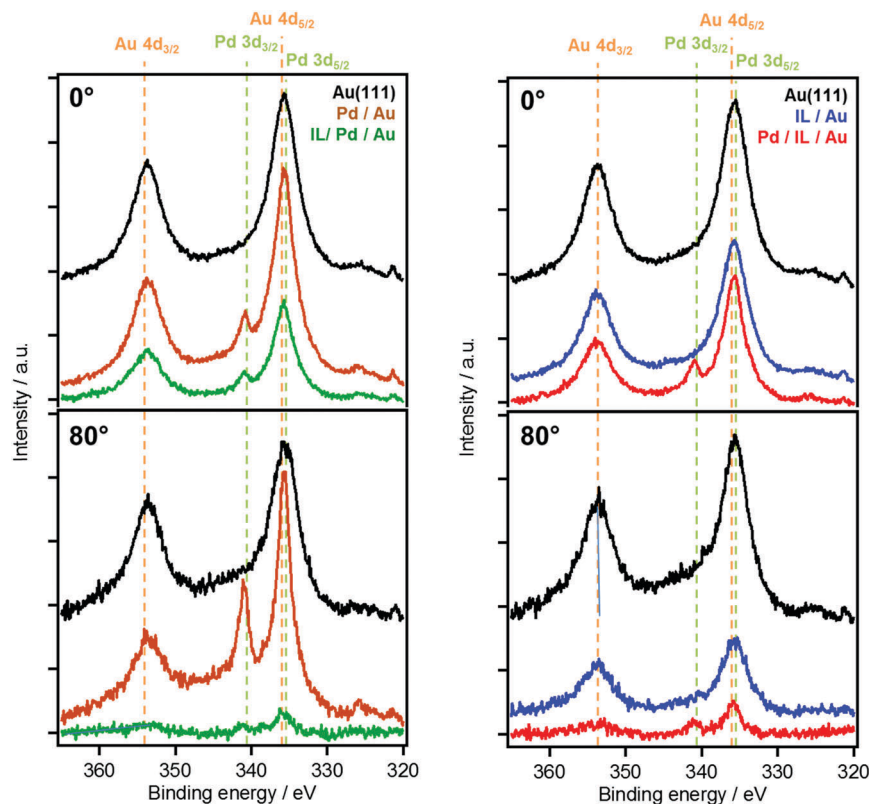
Fig. 2 Bulk sensitive 0° (first row) and surface sensitive 80° (second row) spectra of the Au 4d/Pd 3d region for the sequence 1.6 Å (0.7 ML) Pd on Au(111) followed by deposition of nominally 23 Å (∼3 ML) [C₂C₁Im][OTf] (left column) and the sequence 23 Å [C₂C₁Im][OTf] on Au(111) followed by the deposition of 1.6 Å Pd (right column). All experiments were carried out at RT. Note that the Pd $3d_{5/2}$ signal superimposes with the Au $4d_{5/2}$ signal; thus, only the corresponding discriminable $d_{3/2}$ signals are discussed.

LEIS, XPS and AES study on PVD-deposited Pd on Au(111) in UHV.[27] Segregation of Au to the surface or diffusion of Pd into the subsurface results in pseudomorphic growth of a Pd–Au alloy on Au(111).[27]

The subsequent deposition of nominally 23 Å IL onto the Pd–Au surface alloy leads to a pronounced attenuation of both Au 4d and Pd 3d intensity, as is evident from the green spectra in Fig. 2(left), and the corresponding green squares in Fig. 1. The measured attenuation is very close to that expected for two-dimensional growth (dotted lines), which is attributed to strong interactions of the IL with Pd surface atoms. This contrasts the behavior upon deposition of 23 Å [C₂C₁Im][OTf] onto the pristine Au(111) surface; see blue spectra in Fig. 2(right). This change is also evident from Fig. 1, where the black vertical arrows indicate the enhanced attenuation in case of predeposited Pd.

An overall similar behavior, confirming an attractive inter-action between [C₂C₁Im][OTf] and Pd, is observed in the reverse experiment "Pd/IL/Au", in which first the IL is deposited onto clean Au(111), forming 3D islands on the surface; see blue spectra in Fig. 2(right). Upon subsequent evaporation of Pd, the attenuation of Au substrate signals in the red spectra in Fig. 2(right), in particular at 80°, is significantly stronger than expected from the deposition of only 1.6 Å of Pd on top of the IL. This stronger attenuation is attributed to an increased wetting of the substrate with the IL, induced by the additional presence of Pd.

The transition from 3D islands towards a homogeneous IL film is further supported by an increase of IL signals after Pd deposition, as is exemplarily shown in Fig. 3 for the imidazolium N 1s peak (red vs. blue spectra). The IL signal increase upon Pd deposition is more pronounced in the surface-sensitive 80° emission. The red spectrum at 0° shows a shoulder, shifted to lower BE by 1.8 eV relative to the main peak, which is absent at 80°. It therefore originates not from the IL/vacuum interface but from the buried IL/Au–Pd interface region. The peak could be due to a charge transfer between the [C₂C₁Im]⁺ cation and Pd, leading to a more neutral – possibly carbene-like – species. The tendency of forming carbenes with Pd is known for several catalytic systems carried out in imidazolium-based ILs.[30] Interestingly, this low BE shoulder present for imidazolium cations at the IL–metal interface is only detectable in the sequence "Pd/IL/Au" and is absent for "IL/PD/Au" when the IL is deposited onto the Pd/Au alloy (Fig. 3, green spectra). Apparently, isolated Pd atoms that are only avail-able upon deposition of Pd in the "Pd/IL/Au" experiment are more reactive than Pd atoms already incorporated in the alloy surface.

Notably, for both sequences, that is, "IL/Pd/Au" and "Pd/IL/Au", quantitative XPS analysis on the IL-related signals did not reveal any significant enrichment of any of the measured IL species in surface sensitive 80° emission (not shown), indicating a random distribution of both, anions and cations at the IL/vacuum interface.
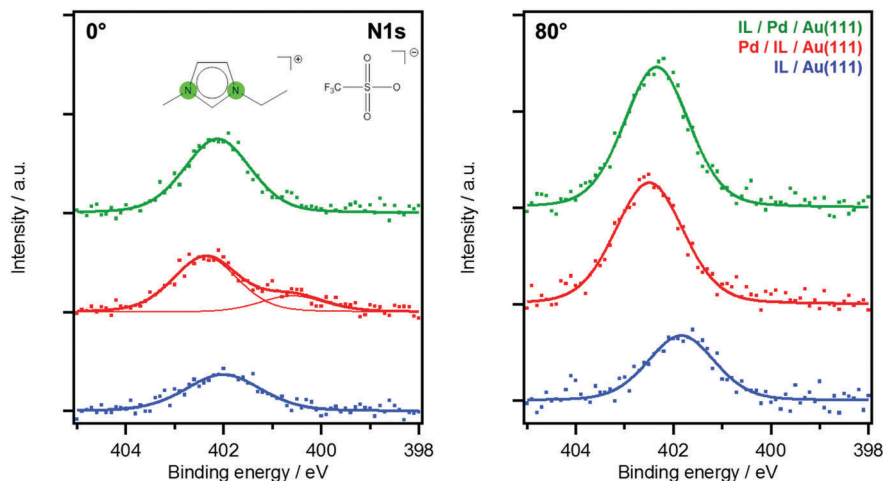
Fig. 3 0° (left) and 80° (right) N 1s spectra of the imidazolium ring N atoms of the two series. Colors correspond to spectra of Fig. 2: deposition of 23 Å IL on Au(111) (blue), followed by Pd deposition (red) in comparison of 23 Å IL deposited onto 1.6 Å Pd/Au(111) (green).

In Fig. 4, a direct comparison of the 0° and 80° spectra of the Au 4d/Pd 3d region after the deposition sequences IL/Pd/Au (green) and Pd/IL/Au (red) is shown. At 0°, the overall intensity of both metal substrate signals is somewhat larger for Pd/IL/Au, due to a less pronounced 2D film formation (wetting) for this deposition sequence. At 80°, in line with the 0° data, the overall intensity is also larger for the Pd/IL/Au sequence, but for the Pd $3d_{3/2}$ signal at 340.5 eV this effect is significantly more pronounced. This enhanced Pd intensity could be an indication for the partial suppression of surface alloying in the presence of the IL for the Pd/IL/Au sequence, possibly due to the strong interactions of single Pd atoms with $[C_2C_1Im]^+$ cations discussed above. In the context of heterogeneous catalysis using the SCILL concept, these results directly provide a possible explanation on the molecular level for the beneficial influence of the IL layer in case of heterogeneous metal alloy catalysts.

The different scenarios upon IL deposition on Au(111) and for pre- and postdeposition of Pd are summarized in Fig. 5. The left panel (a) shows the pronounced 3D growth of $[C_2C_1Im][OTf]$ on the bare Au(111) surface (non-wetting situation). The center panel (b) indicates the 2D layer-by-layer IL growth on the PdAu surface alloy created by Pd predeposition (perfect wetting). The right panel (c) shows the situation after Pd postdeposition onto the IL film of panel (a), that is, a pronounced change in IL film morphology from 3D to 2D, with the Pd atoms stabilized at the Au-IL interface. As for predeposited Pd, a transition towards 2D growth is observed, albeit less pronounced. In addition, upon Pd postdeposition, surface alloying of Pd and Au seems to be suppressed, most likely due to a significant interaction of the IL cations with more reactive surface Pd atoms.

An interesting question in this context is, whether surface alloying in the here studied SCILL-type model system is also
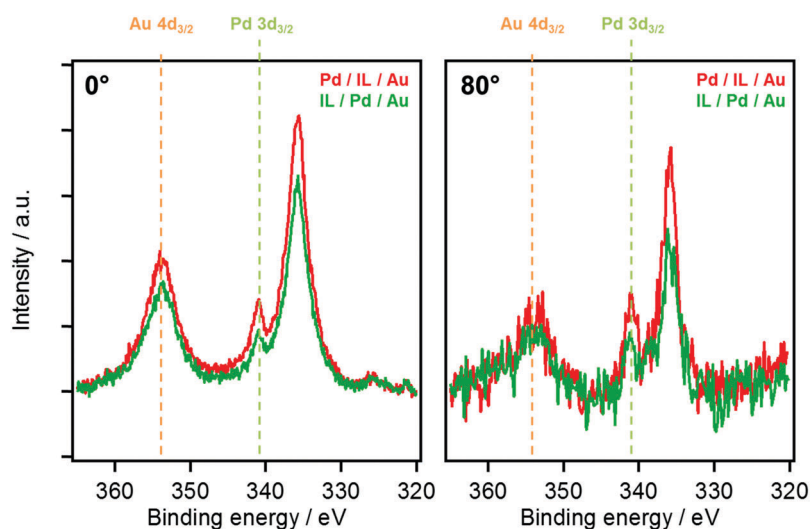

Fig. 4 Direct comparison of the 0° and 80° spectra of the Au 4d/Pd 3d region after the final deposition steps of both sequences, that is, IL/Pd/Au (red) and Pd/IL/Au (green); only core levels unambiguously attributed to Au and Pd are marked and discussed in the text. Note: the 80° spectra have been modified by averaging over two data points to improve signal-to-noise ratio.
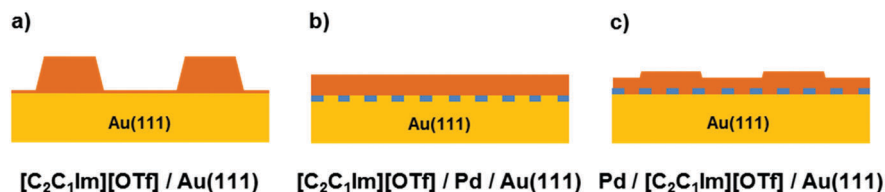
25148 | *Phys. Chem. Chem. Phys.*, 2016, **18**, 25143–25150

This journal is © the Owner Societies 2016

Fig. 5 Scheme of the suggested interface morphologies of (a) [C$_2$C$_1$Im][OTf] deposited onto pristine Au(111), (b) [C$_2$C$_1$Im][OTf] deposited onto a Pd–Au surface alloy (sequence IL/Pd/Au), and (c) deposition of Pd onto the predeposited IL film (sequence Pd/IL/Au). Color code: yellow = Au(111) substrate, orange = [C$_2$C$_1$Im][OTf], blue = Pd atoms.

hindered by an IL film at elevated temperatures, that is, closer to the operation conditions of a real catalyst; this is however out of the scope of the present study, and will be addressed in future experiments. Notably, for the catalytic dehydrogenation of liquid organic hydrogen carriers, we have already shown that UHV model IL systems can come very close to real reaction conditions.[38]

4. Summary and conclusions

In the context of surface science studies on model systems for SCILL catalysts, we investigated the interaction of a model IL adsorbed on clean and modified Au(111) by ARXPS, and evaluated potential routes to switch the growth behavior by pre- or postdeposition of Pd atoms. On clean Au(111), we find that upon thermal deposition of UTIL [C$_2$C$_1$Im][OTf] films in the submonolayer range, the IL adsorbs in a checkerboard arrangement with cations and anions located next to each other. This initial behavior is similar to that observed for [dialkylimidazolium][Tf$_2$N] ILs on the same substrate, where a 2D wetting layer with a thickness of up to 0.5 ML is formed.[18,21] For coverages above 0.5 ML, the onset of pronounced 3D growth occurs. This behavior contrasts the layerwise growth found for [dialkylimidazolium][Tf$_2$N] ILs on Au(111), and is attributed to stronger cation–anion interactions in case of the smaller [OTf]$^-$ anion. By depositing small amounts of Pd before or after the deposition of the IL, a strongly improved wetting behavior was observed. This finding is attributed to attractive interactions between [C$_2$C$_1$Im][OTf] and Pd surface atoms that allow for switching the growth mode from 3D to 2D. For Pd deposition subsequent to the deposition of the IL, the ARXPS data revealed particularly strong interactions between the dialkylimidazolium cation and single Pd atoms, which seem even to be strong enough to prevent surface alloying of Pd and Au, which occurs at RT in absence of the IL.[27] This stabilization mechanism might be one key player in the catalytic cycles of corresponding Pd-containing SCILL catalysts.

Acknowledgements

References

1 T. Welton, *Coord. Chem. Rev.*, 2004, **248**, 2459–2477.

2 T. Welton, *Chem. Rev.*, 1999, **99**, 2071–2084.

3 M. A. B. H. Susan, A. Noda, S. Mitsushima and M. Watanabe, *Chem. Commun.*, 2003, 938–939, DOI: 10.1039/B300959A.

4 J.-P. Belieres, D. Gervasio and C. A. Angell, *Chem. Commun.*, 2006, 4799–4801, DOI: 10.1039/B611150E.

5 P. Wang, S. M. Zakeeruddin, J.-E. Moser and M. Grätzel, *J. Phys. Chem. B*, 2003, **107**, 13280–13285.

6 P. Wang, S. M. Zakeeruddin, P. Comte, I. Exnar and M. Grätzel, *J. Am. Chem. Soc.*, 2003, **125**, 1166–1167.

7 F. Fabregat-Santiago, J. Bisquert, E. Palomares, L. Otero, D. Kuang, S. M. Zakeeruddin and M. Grätzel, *J. Phys. Chem. C*, 2007, **111**, 6550–6560.

8 R. Kawano, H. Matsui, C. Matsuyama, A. Sato, M. A. B. H. Susan, N. Tanabe and M. Watanabe, *J. Photochem. Photobiol., A*, 2004, **164**, 87–92.

9 H.-P. Steinrück and P. Wasserscheid, *Catal. Lett.*, 2015, **145**, 380–397.

10 S. Baldelli, *Acc. Chem. Res.*, 2008, **41**, 421–431.

11 S. Baldelli, *J. Phys. Chem. Lett.*, 2013, **4**, 244–252.

12 B. Uhl, T. Cremer, M. Roos, F. Maier, H.-P. Steinruck and R. J. Behm, *Phys. Chem. Chem. Phys.*, 2013, **15**, 17295–17302.

13 M. Druschler, N. Borisenko, J. Wallauer, C. Winter, B. Huber, F. Endres and B. Roling, *Phys. Chem. Chem. Phys.*, 2012, **14**, 5090–5099.

14 R. Wen, B. Rahn and O. M. Magnussen, *Angew. Chem., Int. Ed.*, 2015, **54**, 6062–6066.

15 H. Li, F. Endres and R. Atkin, *Phys. Chem. Chem. Phys.*, 2013, **15**, 14624–14633.

16 Y. Lauw, M. D. Horne, T. Rodopoulos, V. Lockett, B. Akgun, W. A. Hamilton and A. R. J. Nelson, *Langmuir*, 2012, **28**, 7374–7381.

17 T. Cremer, M. Killian, J. M. Gottfried, N. Paape, P. Wasserscheid, F. Maier and H.-P. Steinrück, *ChemPhysChem*, 2008, **9**, 2185–2190.

18 T. Cremer, M. Stark, A. Deyko, H. P. Steinrück and F. Maier, *Langmuir*, 2011, **27**, 3662–3671.

19 T. Cremer, L. Wibmer, S. K. Calderon, A. Deyko, F. Maier and H. P. Steinruck, *Phys. Chem. Chem. Phys.*, 2012, **14**, 5153–5163.

20 A. Deyko, T. Cremer, F. Rietzler, S. Perkin, L. Crowhurst, T. Welton, H.-P. Steinrück and F. Maier, *J. Phys. Chem. C*, 2013, **117**, 5101–5111.

This journal is © the Owner Societies 2016

Phys. Chem. Chem. Phys., 2016, **18**, 25143–25150 | 25149

21 F. Rietzler, M. Piermaier, A. Deyko, H.-P. Steinrück and F. Maier, *Langmuir*, 2014, **30**, 1063–1071.

22 F. Rietzler, J. Nagengast, H. P. Steinrück and F. Maier, *J. Phys. Chem. C*, 2015, **119**, 28068–28076.

23 P. Zebisch, W. Huber and H. P. Steinrück, *Surf. Sci.*, 1991, **244**, 185–196.

24 J. Greeley and M. Mavrikakis, *Nat. Mater.*, 2004, **3**, 810–815.

25 F. Gao and D. W. Goodman, *Chem. Soc. Rev.*, 2012, **41**, 8009–8020.

26 C. W. Yi, K. Luo, T. Wei and D. W. Goodman, *J. Phys. Chem. B*, 2005, **109**, 18535–18540.

27 B. E. Koel, A. Sellidj and M. T. Paffett, *Phys. Rev. B: Condens. Matter Mater. Phys.*, 1992, **46**, 7846–7856.

28 C. S. Casari, S. Foglio, F. Siviero, A. Li Bassi, M. Passoni and C. E. Bottani, *Phys. Rev. B: Condens. Matter Mater. Phys.*, 2009, **79**, 195402.

29 N. T. S. Phan, M. Van Der Sluys and C. W. Jones, *Adv. Synth. Catal.*, 2006, **348**, 609–679.

30 S. Chowdhury, R. S. Mohan and J. L. Scott, *Tetrahedron*, 2007, **63**, 2363–2389.

31 S. Schernich, D. Kostyshyn, V. Wagner, N. Taccardi, M. Laurin, P. Wasserscheid and J. Libuda, *J. Phys. Chem. C*, 2014, **118**, 3188–3193.

32 T. Bauer, S. Mehl, O. Brummel, K. Pohako-Esko, P. Wasserscheid and J. Libuda, *J. Phys. Chem. C*, 2016, **120**, 4453–4465.

33 R. F. Roberts, D. L. Allara, C. A. Pryde, D. N. E. Buchanan and N. D. Hobbins, *Surf. Interface Anal.*, 1980, **2**, 5–10.

34 I. Niedermaier, C. Kolbeck, H.-P. Steinrück and F. Maier, *Rev. Sci. Instrum.*, 2016, **87**, 045105.

35 A. M. Fernandes, M. A. A. Rocha, M. G. Freire, I. M. Marrucho, J. A. P. Coutinho and L. M. N. B. F. Santos, *J. Phys. Chem. B*, 2011, **115**, 4033–4041.

36 M. Deetlefs, C. Hardacre, M. Nieuwenhuyzen, A. A. H. Padua, O. Sheppard and A. K. Soper, *J. Phys. Chem. B*, 2006, **110**, 12055–12061.

37 A. M. Fernandes, J. A. P. Coutinho and I. M. Marrucho, *J. Mass Spectrom.*, 2009, **44**, 144–150.

38 T. Matsuda, N. Taccardi, J. Schwegler, P. Wasserscheid, H.-P. Steinrück and F. Maier, *ChemPhysChem*, 2015, **16**, 1790.

25150 | *Phys. Chem. Chem. Phys.*, 2016, **18**, 25143–25150

This journal is © the Owner Societies 2016